# Two-Fluid Modeling of the Near-Field of Full-Cone Sprays

Venkatraman Iyer[1], John Abraham[2]

[1]GE Corporate Research and Development, Bldg. K-1, ESB-109, Schenectady, New York
[2]Corresponding Author: Maurice J. Zucrow Laboratories, Purdue University, West Lafayette, IN 47907-2014, USA

**Abstract**

A two-fluid Eulerian-Liquid Eulerian-Gas (ELEG) model is employed to model full-cone sprays. Results are presented in transient and steady sprays. In transient sprays, results of spray penetration and entrainment velocities are presented. In steady sprays, results of liquid-phase penetration, spray angle and entrainment constants are presented. Results are compared with measured results. It is shown that computed transient spray penetration agree with measured results within 10%, entrainment velocities agree within 20%, liquid phase penetration within 25% and entrainment constants and spray angles show the measured trends though quantitative comparisons are more difficult.

## 1. Introduction

The most widely adopted framework for modeling sprays employs a Eulerian approach to the equations governing the gas flowfield and a Lagrangian Monte-Carlo particle tracking approach to solve the equations governing the dynamics of droplets which are often collectively treated as parcels. This framework is intuitively appealing, relatively simple to implement and employing parcels, rather than individual drops, reduces computational time and memory requirements [1-2]. However, the Lagrangian approach has several limitations [3-8]. The gas volume fraction in the computational cell has to be large, i.e. greater than 99%, for the assumptions of the approach to be valid. To enforce this criterion, the smallest grid size that may be employed in the near-orifice region has to be much greater than the orifice radius. This grid size is insufficient to resolve the sharp gradients in the near-orifice region. Furthermore, the Lagrangian approach cannot be employed to represent the intact liquid cone. The modeling of drop-drop interactions assumes that the drops are uniformly distributed in a computational cell. This requirement is difficult to satisfy near the orifice or close to the centerline in the near field of the spray, i.e., within about 100 orifice diameters. Sharp gradients may exist in the droplet distribution that cannot be resolved by the practical grid resolution [5]. As a result, numerically converged results are not obtained with the approach [3-8].

Several alternate approaches to the Eulerian-Lagrangian one have been reported in the literature. In this work, we employ a two-fluid Eulerian-liquid Eulerian-gas (ELEG) model, that we have developed for sprays to compare measured and computed quantities in transient and steady sprays. The numerical limitations highlighted above are minimized with the ELEG approach.

## 2. The Two-Fluid Model

The two-fluid model that is employed here for sprays has been described elsewhere in detail [9]. The essential idea behind the modeling approach is to solve continuum Eulerian equations for the liquid and gas phases. The formulation involves ensemble averaging the local and instantaneous equations for each phase where the independent variables are the spatial coordinates and time. Submodels are employed for the following physics: momentum transfer between the two phases is modeled through a drag correlation; k-ε model is employed to model turbulence; a blob-atomization model is employed to simulate atomization and liquid break-up [10-11]; and, the collisions-coalescence model of O'Rourke and Bracco [2] is employed in which the relative velocity is assumed to be proportional to the local turbulence velocity. The modeling of vaporization, liquid break-up and collision-coalescence involves the solution of an equation for surface area density as described in prior work [12-13]. The equations given above for the ELEG model are supplemented by equations for thermal and caloric equations of state. A finite volume numerical method based on staggered grid and donor-cell convective fluxes is employed to solve the equations above. The method follows the semi-implicit formulation of Patankar and Spalding [14], Liles and Reed [15] and Magi [16].

## 3. The Computational Conditions

We employ three separate sets of experimental data for comparisons with the computed results in this work. In the case of transient sprays, the measurements are those of Naber and Siebers [17], and Cossali et al. [18] and Andriani et al. [19]. The measurements of [17] were made in a pancake-shaped chamber, equipped with quartz windows for full optical access, into which Diesel fuel was injected from the side of the chamber through a single-hole of 0.257 mm diameter. The chamber was filled with nitrogen to prevent combustion. The chamber was pressurized to the desired ambient density. The chamber temperature was about 450 K. The measurements were performed for chamber densities ranging from 3.6 $kg/m^3$ to 124 $kg/m^3$. We will present computed results for the conditions given in Table 1.

Table 1. Experimental conditions for non-vaporizing sprays [17].

| Case | $\rho_a$ $(kg/m^3)$ | $T_a$ (K) | $\rho_f$ $(kg/m^3)$ | $P_f$ (MPa) | $d_o$ mm |
|---|---|---|---|---|---|
| A | 3.6 | 455 | 705 | 138 | 0.257 |
| B | 14.8 | 451 | 705 | 140 | 0.257 |
| C | 60.6 | 451 | 704 | 142 | 0.257 |

Table 2. Injection conditions for entrainment measurements [18, 19].

| | |
|---|---|
| Orifice diameter, d | 0.25 mm |
| Injected mass | 0.306 g |
| Injection duration | 3.3 ms |
| Density of injected fuel $\rho_\ell$ | 820 $kg/m^3$ |
| Average injection velocity $U_{inj}$ | 230 m/s |

Cossali et al. [18] and Andriani et al. [19] studied air entrainment in a transient Diesel spray using LDV to measure gas velocities. The spray was injected into a confined quiescent environment and the entrainment flow rate was evaluated by measuring the air velocity

component normal to a cylindrical surface surrounding the spray. The injection conditions in the measurements are summarized in Table 2. The closed cylindrical chamber had an internal diameter of 206 mm, with injection along the axis of the cylinder. The average mass of fuel injected was obtained as 0.0306 g per injection. Cossali et al. [18] estimated the injected mass flow rate as a function of time from the total mass injected, the injection duration and the measured injection pressure history. Figure 1 shows the estimated injected mass flow rate as a function of time during the period of injection. Measured ambient conditions considered are given in Table 3. Each case given in Table 3 has a different combination of ambient temperature and density. The objective of choosing the conditions given in Table 3 is to study the independent effects of ambient temperature and ambient density on the entrainment characteristics.

Table 3. Ambient conditions for entrainment measurements [18, 19].

| Case | Temperature (K) | Density kg/ $m^3$ |
|---|---|---|
| 1 | 298 | 7.02 |
| 2 | 413 | 5.06 |
| 3 | 298 | 1.17 |
| 4 | 298 | 5.06 |
| 5 | 473 | 5.06 |

Table 4. Experimental conditions for measurements of steady liquid penetration [20].

| | |
|---|---|
| Orifice diameter | 0.246 mm |
| Injection pressures | 65, 90, 120, 136, 170 Mpa |
| Injection velocities | 334, 393, 454, 483, 540 m/s |
| Ambient densities | 3.6, 7.3, 14.8, 30.2, 60 kg/ $m^3$ |
| Fuel temperature | 438 K |

We will also present results of liquid penetrations in vaporizing sprays. The measured liquid penetrations for vaporizing sprays shown are those obtained by Siebers [20]. The measurements were made in a constant volume cubical shaped chamber. The dimension of the cube was 108 mm. Investigation of liquid-phase fuel penetration in Diesel sprays was conducted in inert, high-temperature, high-density conditions generated in the constant-volume vessel. The injection and chamber condition are given in Table 4.

## 4. Results and Discussion

The computational grid employed for the computation is shown in Fig. 2. The computational domain employed in all cases is axisymmetric and has constant volume.

Figure 3, shows the penetration as a function of time for Cases A, B and C of Table 1. The computed penetration shows agreement within 2% of the measurements for the three cases. The penetration increases linearly with time initially, before 0.4 ms after start of injection (ASI), and then shows a $\sqrt{t}$ behavior. This is consistent with previous findings [4].

In the case of vaporizing sprays, the liquid-phase will penetrate to a steady distance within a short duration relative to the duration of injection. The vapor will continue to penetrate farther with time. Figure 4 shows the steady liquid penetration as a function of chamber density,

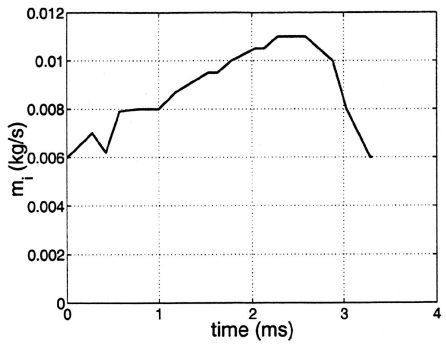


Figure 1. Injected mass flow rate vs. time. Measurements of Cossali et al. (1996).

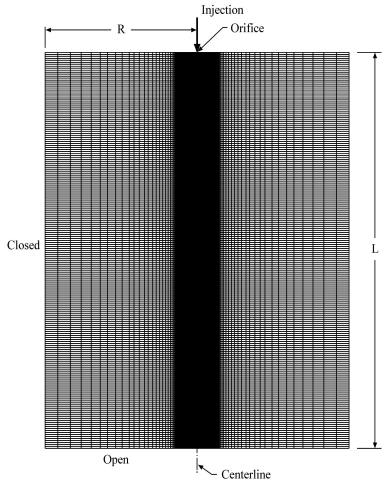


Figure 2. Computational grid.

computed with the model. The results are sensitive to the atomization model constant. The computations are performed with two values of a model constant, $B_1$ [11]. The computed and measured penetrations differ by about 35-40% at the lower ambient densities of 3.3 and 7.2 kg/m$^3$ when $B_1 = 10$ is used. The computed steady liquid penetrations agree within the 10-20% for the ambient density range of 3.3-14.8 kg/m$^3$ when the value of $B_1$ is increased to 20. The penetrations at the higher ambient densities of 30.2 and 60 kg/m$^3$ are greater than the measured values by about 20-30%. However the overall trend is closer to the measurements when $B_1 = 20$. Both values of $B_1$ that we have employed are within the range of 10-60 as suggested by Beale and Reitz [11]. The uncertainty in the value of $B_1$ reflects the lack of understanding of the physics of atomization.

Figure 5 shows the computed steady liquid penetration as a function of injection pressure for ambient densities of 7.02 and 30.2 kg/m$^3$. The figure shows that the steady liquid penetration is approximately constant as injection pressure is changed. This trend is in agreement with the measurements. This behavior is also consistent with the liquid vaporization being mixing-controlled rather than being controlled by individual drop vaporization, i.e. the characteristic time of drop vaporization is much smaller than the characteristic time of mixing [12].

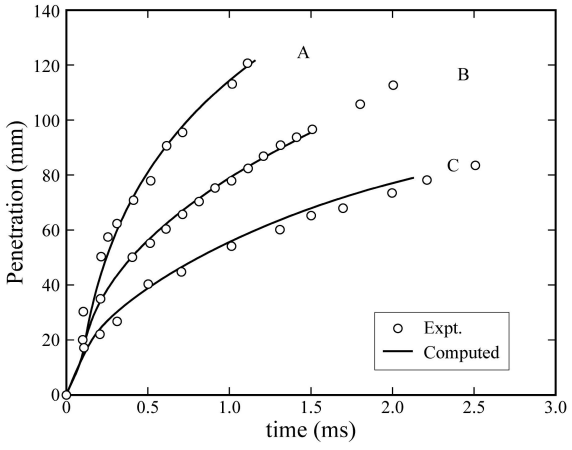


Figure 3. Non-vaporizing spray penetration: comparison of two-fluid computations with measurements.

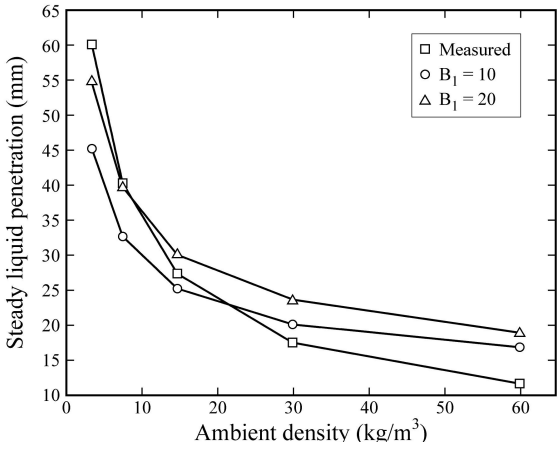


Figure 4. Steady liquid penetration vs. ambient density: $P_{inj}$=136 MPa, $T_a$=1000 K, $d_{orif}$=246 microns.

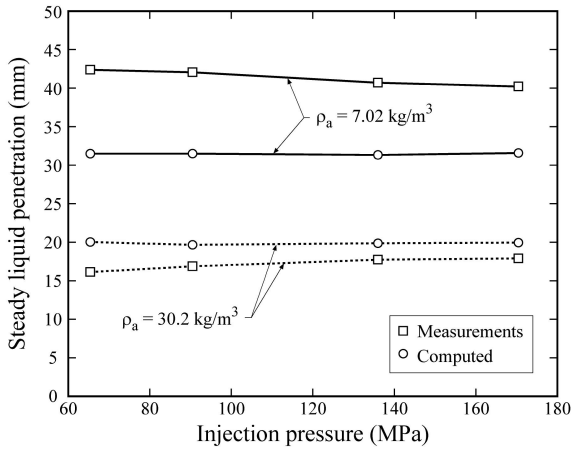


Figure 5. Steady liquid penetration vs. injection pressure: $T_a$=1000 K, $d_{orif}$=246 microns.

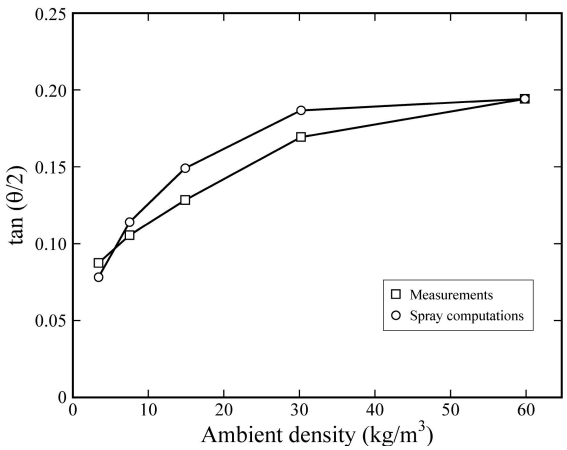


Figure 6. Dispersion angle vs. ambient density: computed and measured vaporizing sprays: $P_{inj}$=136 MPa, Ta=1000 K, $d_{orif}$=246 microns.

Naber and Siebers [17] also measured the spray dispersion angle using a Schlieren imaging system. In a prior study, Iyer and Abraham [4] performed gas jet computations for the same conditions as in the measurements and compared the computed gas jet dispersion angles with the measured dispersion angles. For computing the dispersion angle, we need to define the boundary of the jet [4,17]. The boundary is defined as the locus of points having a fixed value of the fuel density. The selected threshold fuel density was kept constant for all the different chamber density cases. This method of describing the jet boundary was used by Iyer and Abraham [4] for the gas jet computations. Figure 6 shows the computed and measured dispersion angles for the sprays. The angle increases with chamber density as in the measurements. The quantitative values will however be dependent on the threshold value as discussed by Iyer and Abraham [4]. Cossali et al. [18] and Andriani et al. [19] measured the radial velocity of the gas at a radius of 10 mm from the centerline and defined the measured velocity as the entrainment velocity, $V_e$. The radius of 10 mm was chosen as a compromise between the difficulties in measuring velocities too close to the centerline and the large relative errors in the radial velocities with increasing radial distance from the centerline. Figure 7 shows the computed and measured entrainment velocity as a function of time for Case 1 of Table 3. The entrainment velocity is shown for three different axial locations x = 22.5 mm, x = 32.5 mm and x = 57.5 mm. The figure shows that for the three axial locations the computed and the measured entrainment velocities start decreasing to negative values after an initial period of zero entrainment velocity. The decrease is associated with the passage of the head vortex of the jet where the gas tends to be pushed radially outwards by the incoming liquid jet. The velocity reaches a maximum negative value for all the axial locations shown and then starts increasing. The entrainment velocity then becomes positive, which implies that the head vortex has passed the axial location considered and the jet is now entraining the ambient gas at that location. It appears from Fig. 7 that the computed maximum negative entrainment velocity increases with increase in axial location for the axial locations considered. This implies that the strength of the head vortex as measured by the velocity with which the gas is pushed out, increases as the vortex travels downstream from the orifice [19]. Once the jet starts entraining, the velocity increases with time and reaches a steady value before the end of injection at 3.3 ms as shown by the computations in

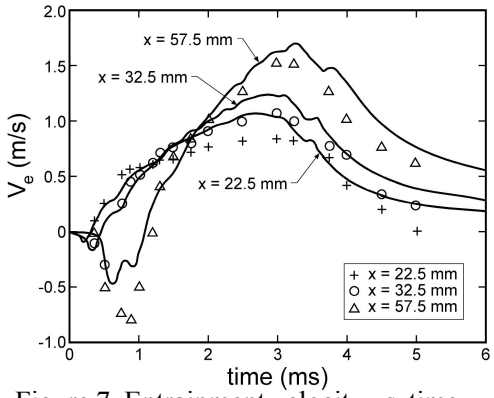


Figure 7. Entrainment velocity vs. time computed with measured injection rate profile for Case 1: +, ○, △; — computed.

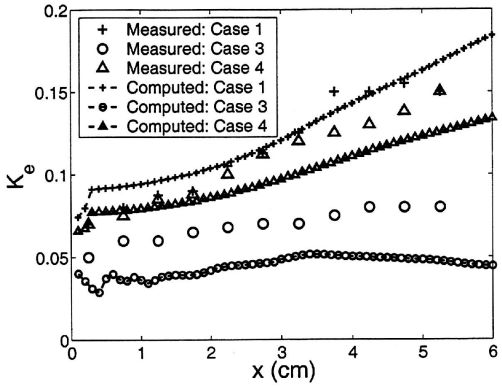


Figure 8. Entrainment constant vs. axial distance: computed and measured: effect of ambient density.

Fig. 10. The computed steady entrainment velocity increases with increase in axial location. The measurements and computed results show the same trend. The steady velocities at x = 57.5 mm and x = 32.5 mm appear to agree with the measurements within 15% and the steady velocity at x = 22.5 mm appears to agree within 20-25%.

The entrainment constant, $K_e$, is a non-dimensional entrainment rate and is defined at a given location, x, as

$$K_e = \frac{d\dot{m}_e(x)}{dx} \frac{d}{\dot{m}_i} \left( \frac{\rho_\ell}{\rho_a} \right)^{1/2} \tag{1}$$

where $\dot{m}_e$ is the total mass flow rate of the entrained gas across the cross-section of the jet at axial location, x. d is the orifice diameter. $\dot{m}_i$ is the injected mass flow rate. $\rho_\ell$ and $\rho_a$ are the injected and ambient densities respectively. $d\dot{m}_e(x)/dx$ may be written as $2\pi r \rho_a V_e$ [21]. Notice that the entrainment constant as defined by Eq. (2) is relevant only in the steady portion of the jet.

Computations are performed to evaluate the effect of ambient density on the entrainment constant in sprays. The ambient conditions corresponding to Cases 1, 3 and 4 are chosen for this purpose. All these cases have the same ambient temperature of 298 K but different ambient densities. Figure 8 shows the computed and measured entrainment constant as a function of the axial distance from the orifice for Cases 1, 3 and 4. The computed values are averaged in the time interval between 2 and 3 ms after start of injection, i.e. once steady values are reached. The figure shows that the measured entrainment constant decreases with decrease in ambient density at all the axial locations shown. The computed entrainment constant shows a similar trend. Decrease in ambient density increases the drop sizes and the break-up length. So the transfer of momentum from the liquid to the gas is slower as the ambient density is decreased. So it is expected that the entrainment constant in the near field decreases with decreasing ambient density. The quantitative agreement between the measurements and the computations is good for Case 1. However for Cases 3 and 4, the computations appear to underpredict the entrainment constant by more than 40% at all the axial locations shown. This may be due to uncertainties in our knowledge of atomization and break up processes in Diesel sprays and it requires more theoretical and experimental investigations.

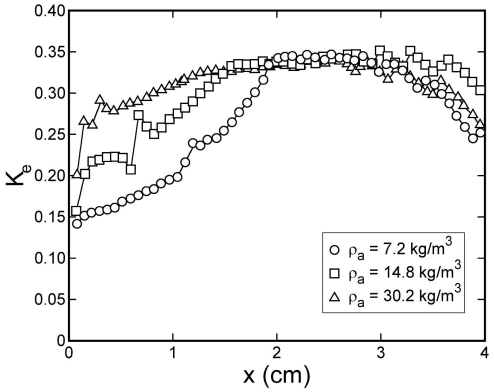


Figure 9. Computed entrainment constant vs. axial distance for vaporizing sprays: effect of ambient density.

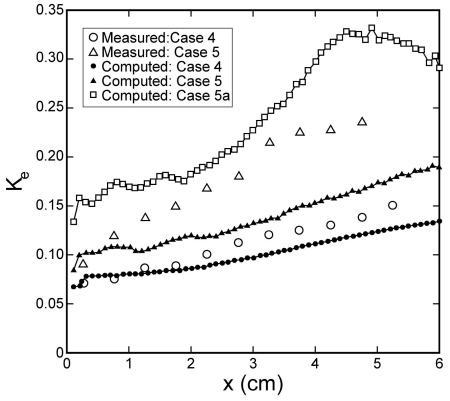


Figure 10. Entrainment constant vs. axial distance: computed and measured: effect of ambient temperature.

It should be noted that the measurements of Cossali et al., [18] are for ambient densities that are lower than those in Diesel engines near top dead center. Also, the measurements are for non-vaporizing sprays. It would be of interest to investigate the behavior of the entrainment constant for vaporizing Diesel sprays for different ambient densities. There are no reported measurements of entrainment constant in vaporizing Diesel sprays to our best knowledge. So we can only look at the computed entrainment constant under these conditions. Figure 9 shows the computed entrainment constant as a function of the axial distance from the orifice for three ambient densities. The cases correspond to the measurements performed at the Sandia National Laboratories for vaporizing sprays where the ambient temperature is about 1000K [17]. Figure 9 shows that the entrainment constant increases with axial distance in the near field for all the cases. However, for the two higher ambient densities, $K_e$ reaches a steady value of about 0.32 within 1.5-2.0 cm i.e., about 15 effective diameters downstream of the orifice. The value of 0.32 is approximately the value of the entrainment constant in steady gas jets as shown in prior works [21]. For lower ambient densities the steady value is reached at a further downstream location and the value of $K_e$ in the near field is lower. A steady entrainment constant was not obtained in the measurements of Cossali et al. [18], because of the low ambient densities and also because of the fact that the measurements were confined to the near field.

Figure 10 shows the computed and measured entrainment constant as a function of the axial distance from the orifice for Cases 4 and 5 of Cossali et al. [18] shown in Table 3. Both these cases have the same ambient density of 5.6 kg/ m$^3$ but Case 4 has an ambient temperature of 298 K whereas Case 5 has an ambient temperature of 473 K. The figure shows that the measured entrainment constant for Case 5 is greater than that for Case 4 by as large as a factor of 2 at the axial location of 4 cm from the orifice. The computations also predict an increase in the entrainment constant when the ambient temperature is increased from 298 K in Case 4 to 473 K in Case 5 but by only about 30%. This difference may arise from inadequate vaporization rates when employing tetradecane as the representative fuel for Diesel in the computations. Figure 10 shows the entrainment constant when octane, which is more volatile than tetradecane, is employed as the fuel (Case 5a). A significant increase in the entrainment constant is predicted. In fact, the behavior of the entrainment constant for Case 5a is similar to that in vaporizing Diesel sprays as shown in Fig. 9 in that $K_e$ approaches a steady value in the range of 0.3-0.33. Thus it appears that the increase in the entrainment constant with increase in the ambient

temperature may be due to the vaporization of the fuel. It is possible that the Diesel fuel used in the measurements might have had some volatile components that vaporizes at 473 K.

## 5. Summary and Conclusions

A two-fluid Eulerian-liquid Eulerian-gas model is employed to study the structure of Diesel sprays. It is shown that the model is able to reproduce measured trends in transient spray penetrations, entrainment velocities in transient sprays, entrainment constants in the near field of steady sprays and steady liquid penetration in vaporizing Diesel sprays. It is shown that the entrainment constant increases from a relatively low value in the near-field to a steady value of about 0.32 at a distance downstream where value is dependent on chamber density and temperature. A lack of understanding of atomization is the serious limitation in clarifying the physics of the near field.

## 6. References


[1] Duckowicz J K 1980 *J. Comp. Phys*. **35(2)** 229-253
[2] O'Rourke P J and Bracco F V 1980 *Inst. Mech. Engines,* Publication 1980-9
[3] Abraham J 1997 *SAE Trans*. **106** 141-155
[4] Iyer V A and Abraham J 1997 *Combust. Sci. Tech.* **130** 315-335
[5] Aneja R and Abraham J 1998 *Combust. Sci. Tech*. **138** 233-255
[6] Subramaniam S and O'Rourke P J 1998 *Los Alamos Lab. Rept.* UR-99-5465
[7] Post S and Abraham J 2001 *Combust. Sci. Tech*. **165** 1-90
[8] Post S L and Abraham J 2002 *Int. J. Multiphase Flow* **28** 997-1019
[9] Iyer V A 2001 Modeling of Diesel Sprays Using an Eulerian-Liquid Eulerian-Gas Two Fluid Model, Ph D Dissertation, Purdue University, West Lafayette, IN
[10] Reitz R D 1987 *Atomization and Spray Tech*. **3** 309-337
[11] Beale J C and Reitz R D 1999 *Atomization and Sprays* **9** 623-650
[12] Iyer V A Post S L Abraham J 2000 *Proc. Comb. Inst*. **28** 1111-1118
[13] Iyer V A Magi V Abraham J 2002 *Int J Heat Mass Transfer* **45** 519 531
[14] Patankar S V and Spalding D B 1972 *Int. J. Heat Mass Transfer* **15** 1787-1806
[15] Liles D R and Reed W H 1978 *J. Comp. Phys*. **26** 390-407
[16] Magi V 1987 *MAE Report No. 1793* Princeton University Princeton NJ
[17] Naber J D and Siebers D L 1996 *SAE Paper 960034*
[18] Cossali G E Berlaano A and Coghe A 1996 *SAE Paper 960862*
[19] Andriani R Coghe A and Cossali G 1996 *Proc. Comb. Inst.* **26** 2549-2556
[20] Siebers D L 1998 *SAE Paper 980809*
[21] Post S L Iyer V A Abraham J 2000 *J. Fluids Engrg*. **122** 385-395